Applied Energy 262 (2020) 114370

Contents lists available at ScienceDirect

Applied Energy

journal homepage: www.elsevier.com/locate/apenergy

# Flexible thermoelectric generators for body heat harvesting – Enhanced device performance using high thermal conductivity elastomer encapsulation on liquid metal interconnects

Yasaman Sargolzaeiaval[a], Viswanath Padmanabhan Ramesh[a], Taylor V. Neumann[b], Veena Misra[a], Daryoosh Vashaee[a], Michael D. Dickey[b], Mehmet C. Öztürk[a,*]

[a] Department of Electrical and Computer Engineering, NC State University, Raleigh, NC, USA
[b] Department of Chemical and Biomolecular Engineering, NC State University, Raleigh, NC, USA

## HIGHLIGHTS

- Liquid metal interconnects encapsulated with a high thermal conductivity elastomer.
- Flexible, body-worn thermoelectric generators with best-in-class performance.
- Highest reported power density > 35 μW/cm$^2$ from body heat harvesting.
- First flexible thermoelectric generator that has the potential to rival rigid TEGs.

## ARTICLE INFO

*Keywords:*
Thermoelectric generators
Body heat harvesters
Flexible electronics
Thermally conductive polymers

## ABSTRACT

This paper reports flexible thermoelectric generators (TEGs) employing eutectic gallium indium (EGaIn) liquid metal interconnects encased in a novel, high thermal conductivity (HTC) elastomer. These TEGs are part of a broader effort to harvest thermal energy from the body and convert it into electrical energy to power wearable electronics. The flexible TEGs reported in this paper employ the same thermoelectric legs' used in rigid TEGs, thus eliminating the need to develop new materials specifically for flexible TEGs that often sacrifice the so-called figure of merit' for flexibility. Flexible TEGs reported here embed rigid thermoelectric legs' in soft and flexible packaging, using stretchable EGaIn interconnects. The use of liquid metal interconnects provides ultimate stretchability and low electrical resistance between the thermoelectric legs. The liquid metal lines are encased in a new stretchable silicone elastomer doped with both graphene nano-platelets and EGaIn to increase its thermal conductivity. This high thermal conductivity elastomer not only reduces the parasitic thermal resistance of the encapsulation layer but it also serves as a heat spreader, leading to 1.7X improvement in the output power density of TEGs compared to devices fabricated with a conventional elastomer. The device performance is further improved by a thin Cu layer acting as a heat spreader providing an additional 1.3X enhancement in the output power at 1.2 m/s air velocity (typical walking speed). Worn on the wrist, our best devices achieve power levels in excess of 30 μW/cm$^2$ at an air velocity of 1.2 m/s outperforming previously reported flexible TEGs.

## 1. Introduction

The wearable electronics industry is growing rapidly with many promising applications in health and performance monitoring systems. The “holy-grail” of wearable devices is long-term, continuous monitoring using the human body as a continuous supply of energy to either achieve self-powered operation or to significantly extend the battery lifetime. Such devices can include many sensors to monitor human health and the environment to achieve a comprehensive understanding of the human condition. Long-term monitoring can significantly improve out-patient treatment following a surgical operation as well as management of chronic diseases such as asthma and diabetes, which can ultimately lead to improvement in quality of life. Yet, the necessity to recharge the batteries in such devices forces the user to periodically remove the device. At best, this results in missed measurement opportunities, and at worst, can cause non-compliance.

* Corresponding author.
*E-mail address:* mco@ncsu.edu (M.C. Öztürk).

https://doi.org/10.1016/j.apenergy.2019.114370
Received 6 September 2019; Received in revised form 3 December 2019; Accepted 12 December 2019
Available online 30 January 2020
0306-2619/ © 2019 Published by Elsevier Ltd.

To realize a fully self-powered operation, the system must rely solely on the energy harvested from the human body or the environment. Previous studies focused on body heat [1–10], body motion [11–16], and wireless RF [17–21] as potential energy sources. Among these, harvesting the body heat using thermoelectric generators (TEGs) emerges as a promising solution since heat is available continuously even when the body is at rest. A typical thermoelectric generator consists of P-type and N-type semiconductor legs sandwiched between two thermally conductive headers, and metal traces that electrically interconnect the legs in series. As such, the legs of a TEG are thermally in parallel and electrically in series. When a TEG is placed on a heat source (e.g. human body), heat flows through the legs developing a temperature differential, ΔT, between the two headers. Each leg generates a voltage determined by the temperature differential and the Seebeck coefficient of the thermoelectric material. Since the polarities of the voltages generated across the P- and N-type legs are opposite, they add to produce a larger output voltage. A heatsink is typically attached to the cold side to encourage heat rejection and to achieve a larger temperature differential across the legs. Bismuth chalcogenides are proven to be the most efficient materials at typical body temperatures.

The interest in flexible TEGs as body heat harvesters is growing due to their ability to conform to the human skin and their potential to provide an aesthetically pleasing system in the form of an elastic band [1,22]. Flexible TEGs also have the potential to find use cases in industrial applications where they can conform to non-flat surfaces (in contrast, conventional TEGs are built from rigid materials that cannot bend). Previous work on flexible TEGs explored a variety of different processes to deposit both organic and inorganic thermoelectric materials on flexible substrates using a variety of techniques including physical vapor deposition, screen printing and electrochemical deposition [23–42]. Another approach followed by different groups focused on encasing rigid thermoelectric legs in a stretchable elastomer [4,6–9,43,44]. It is quite challenging to compare these devices since the characterization methods and conditions exhibit considerable variations between different laboratories. Nevertheless, Fig. 1 attempts to compare the power densities of recently reported flexible TEGs as a function of ΔT across the device for $\Delta T < 30^{\circ}C$. We note that some of the data points in Fig. 1 were calculated based on the reported parameters (such as voltage, surface area, and temperature) in the papers. We can see that with the exception of a few, the power densities of the flexible TEGs included in this summary is below 10 $\mu W/cm^2$. Therefore, there is a strong need to develop technologies that can deliver at least an order of magnitude higher power density to make this approach feasible for wearable devices, which will typically require hundreds of microwatts to operate.

This laboratory previously proposed a unique approach to fabrication of flexible TEGs. The approach relies on rigid thermoelectric legs (i.e. the same legs used in rigid TEGs) connected in series using stretchable, self-healing eutectic gallium-indium (EGaIn) liquid metal interconnects encased in a stretchable elastomer [8,45]. A similar TEG with rigid thermoelectric legs and galinstan interconnects was also reported by Jeong et al. [9]. More recently, Chen et al. reported a lateral TEG [46], which also employed EGaIn interconnects. In this device, nanowires of thermoelectric material were inkjet printed on a kapton substrate and connected in series using EGaIn interconnects. While inkjet printing of the material is intriguing, more work is needed on this approach to match the properties of bulk thermoelectric materials. More importantly, this device is not suitable for wearable devices due its planar geometry. With a resistivity of 2.94 μΩ·cm, the EGaIn interconnects' contribution to the device resistance is negligibly small [47]. Furthermore, EGaIn is non-toxic and does not evaporate [48,49], an important advantage for wearable applications. The device developed in this work is effectively soft, flexible, and stretchable since all of the materials are soft, other than the small, rigid thermoelectric 'legs'. One potential issue with Ga is that it can alloy with metals like Bi and Sb [50,51]. However, the devices fabricated in this study maintained their

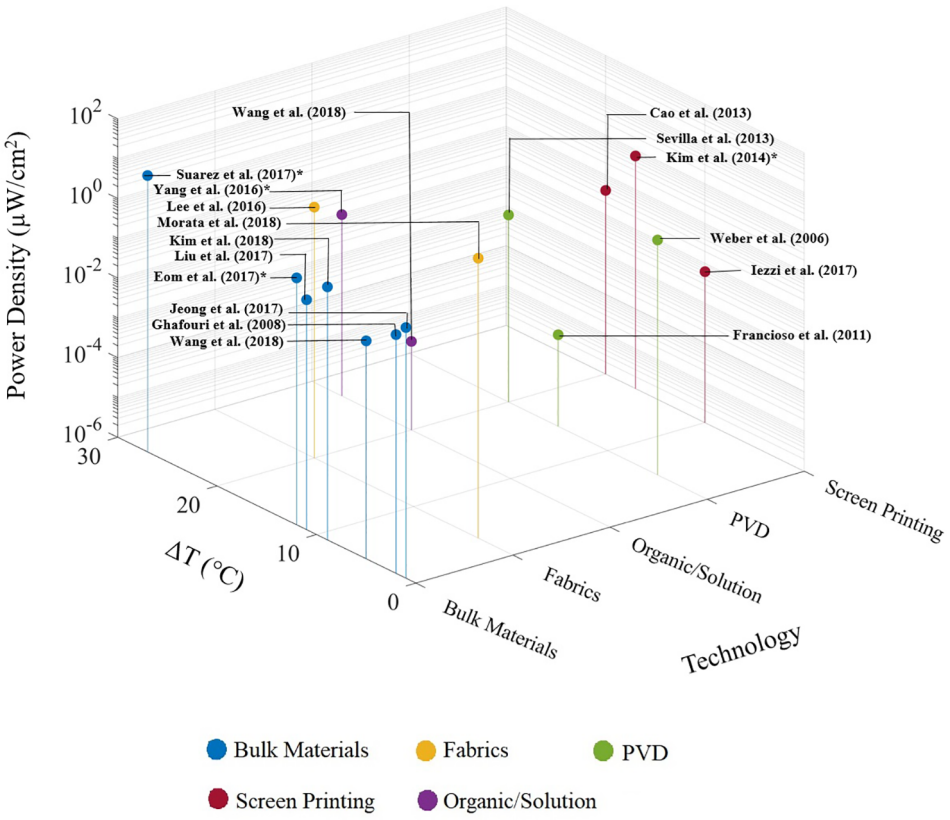


**Fig. 1.** A comparison of generated power levels for some of the recent flexible thermoelectric generators created to date. (*On-body measurement).

total resistance and overall performance with no noticeable changes within a period of one year suggesting that neither the electrical contact resistivity nor the thermoelectric properties were not affected. It is also important to note that Ga is not in direct contact with the thermoelectric material due to several layers of contact metallization including Au and Ti. Finally, the total weight of EGaIn used in the TEGs reported here (for both interconnects and encapsulation layers) is around 175 mg/cm$^2$ which would cost less than \$0.2/cm$^2$, which is negligible compared to the cost of the thermoelectric legs.

The proof-of-concept TEGs reported by Suarez et al. exhibited performance levels, which suggested that it might be possible to produce flexible TEGs that rival the performance of their rigid counterparts [8]. A key attraction of this approach is its compatibility with the thermoelectric legs used in rigid devices, which eliminates the need to develop new flexible thermoelectric materials that often sacrifice performance to gain flexibility. Furthermore, the fabrication process is compatible with pick-and-place tooling used in rigid TEG manufacturing. As such, these attributes make the technology quite accessible to manufacturers of rigid thermoelectric modules.

A key challenge in using liquid metal interconnects in flexible TEGs is that liquid EGaIn interconnects need to be encapsulated. It is sensible to encase the metal in a silicone elastomer because silicones are generally easy to process and have soft mechanical properties. Because the temperature differential between the skin and the surrounding environment is small (typically less than 10°), it is imperative that this encasing layer can provide a sufficiently high thermal conductivity to minimize its contribution to the parasitic thermal resistance on both sides of the device. Recently, this group has reported a method to increase the thermal conductivity of polydimethylsiloxane (PDMS) by 5.6X by adding EGaIn droplets and graphene nano-platelets to the elastomer. The focus of this report is flexible TEGs with EGaIn interconnects fabricated using this new high thermal conductivity (HTC) encapsulation material. The results show that the best devices incorporating the new elastomer can deliver power density levels above 10 μW/cm$^2$ rivaling the performance of the best rigid TEGs used for heat harvesting from the human body. Compared to other previously reported flexible TEGs, wearable TEGs developed in this study demonstrate the highest power density levels measured on the human body, which will be reviewed in the Results“ section.

## 2. Experimental

Fig. 2 shows the process flow used to fabricate the flexible TEGs. The P-type and N-type thermoelectric legs (0.7 mm × 0.7 mm × 3 mm), acquired from a commercial supplier, are composed of $Bi_{0.5}Sb_{1.5}Te_3$ and $Bi_2Se_{0.3}Te_{2.7}$ respectively. The legs were received with Au contacts on either side of the legs. The properties of these legs are summarized in Table 1. The leg dimensions were optimized using the quasi-3D model reported in a previous paper by this group [52]. The aspect ratio of the legs was chosen such that the intrinsic thermal resistance of the TEG is sufficiently large relative to the parasitic thermal resistances, which include the EGaIn encapsulation resistance, contact resistances at the TEG/skin and TEG/air interfaces and the thermal resistance of the human skin.

The thermoelectric legs were first placed on a glass slide through a stencil (Fig. 2a). A double-sided adhesive tape was used to secure the legs on a glass slide. Polydimethylsiloxane (PDMS, Slygard™ 184, Dow Corning) silicone elastomer with a base to curing agent ratio of 10:1 was poured between the legs, planarized and cured. PDMS was mixed in a mixing and degassing machine (THINKY, ARE-250) before casting (Fig. 2b). Planarization involved placing a second glass slide (with a thermal release tape) on top of the legs to help keep the surface level and smooth. After curing the silicone at 70°C for 2 h on a hotplate, the hotplate temperature was elevated to 90°C to remove the thermal release tape and the planarizing glass slide. Any PDMS residue on the legs was manually removed under a microscope. EGaIn interconnects were sprayed on the device through another stencil made of wax paper. Wax paper was preferred since it allowed easy removal of the stencil without damaging the interconnect lines. EGaIn spray coating was carried out for 5 s from a distance of approximately 10 cm (Fig. 2c) to achieve a thickness of 200 μm. Compared to the stencil-printing method used in the fabrication of our earlier devices [8], spray coating greatly simplified EGaIn application and significantly improved the device yield. Specifically, the technique eliminated the need to (i) pre-wet the legs with EGaIn and HCl to remove the skin oxide on the EGaIn surface, and, (ii) oxygen plasma treatment of the PDMS surface for successful wetting by EGaIn. Another important advantage of spray coating is that it allowed us to increase the leg density by reducing the separation between the interconnects. The leg density is commonly quantified using the TEG fill factor, which refers to the area occupied by the legs relative to the device total area. Using spray coating of EGaIn, we were able to successfully increase the fill factor from 5% used in our proof-of-concept devices to 20%. The EGaIn interconnects were then encapsulated by spraying a thin (~50 μm) layer of PDMS. This layer secured the interconnects and provided easy handling of the device in subsequent steps. To spray the elastomer, PDMS was diluted with hexane using a weight ratio of 1:1. The spray coating was carried out for 10 s and the sprayed elastomer was cured on a hotplate at 140°C for approximately 15 min (Fig. 2d). The TEG was then flipped and the same steps were repeated on the back side of the device to complete the electrical circuit (Fig. 2e). The TEGs were then coated on both sides with the HTC elastomer to increase the thickness of the encapsulation layer and increase the structural integrity of the final device. The elastomer was cured for 2 h at 70°C on a hotplate (Fig. 2f).

To produce the HTC elastomer, equal amounts (by weight) of PDMS and EGaIn (Sigma Aldrich) (14% EGaIn by volume) were shear mixed in a THINKY ARE-250 planetary mixer. Shear mixing reduces the size of the liquid metal droplets, which retains their shapes after curing the composite [53]. Immediately after mixing, GnPs with an average diameter of 25 μm (Sigma Aldrich 900413) were mixed into the elastomer using a weight percentage of 2.2%. The results of an in-depth study on the thermal and mechanical properties of this HTC elastomer can be found in a recent publication by this group [54]. Fig. 3 shows the reported thermal conductivity of the elastomer as a function of the GnP weight percentage included in this paper for continuity. The thermal conductivity of pure PDMS with no EGaIn is also included as a reference. We can see that the thermal conductivity is enhanced by both EGaIn and GnP addition to the elastomer. With EGaIn and 2.2% GnP inclusion, the thermal conductivity of the elastomer is 0.84 W/mK corresponding to a 5.6X enhancement of the PDMS thermal conductivity. Since the improvement in thermal conductivity beyond this concentration is small, we have chosen to use this concentration to fabricate our TEGs. At 2.2%, the material is still quite flexible and stretchable as shown in the insert of Fig. 3. Fig. 4 shows the cross-sectional microscope image of a typical TEG with HTC elastomer encapsulation. TEGs with different encapsulation thicknesses and fill factors were fabricated to study the impact of the encapsulation elastomer on device performance via experiments and modeling.

TEGs were also fabricated with thin copper heat spreaders deposited on the HTC elastomer. DC Sputtering was used to deposit a 30 nm Ti layer on the elastomer as an adhesion promoter. This was followed by the deposition of a 300 nm thick copper layer to serve as the seed layer for electroplating an 8 μm thick copper layer in a copper sulfate solution using a current density of 0.02 mA/cm$^2$ Higher current densities were found to etch the seed layer, resulting in chipping or complete removal of the electroplated metal.

The fabricated TEGs were characterized using the measurement setup shown in Fig. 5a. A hotplate kept at 32°C was used as the heat source. The “wind tunnel“, shown in Fig. 5, was designed and fabricated using a resin 3D printer. We used an adjustable speed electric fan to create airflow through the tunnel and an anemometer was placed directly over the TEG to measure the air velocity. The ambient

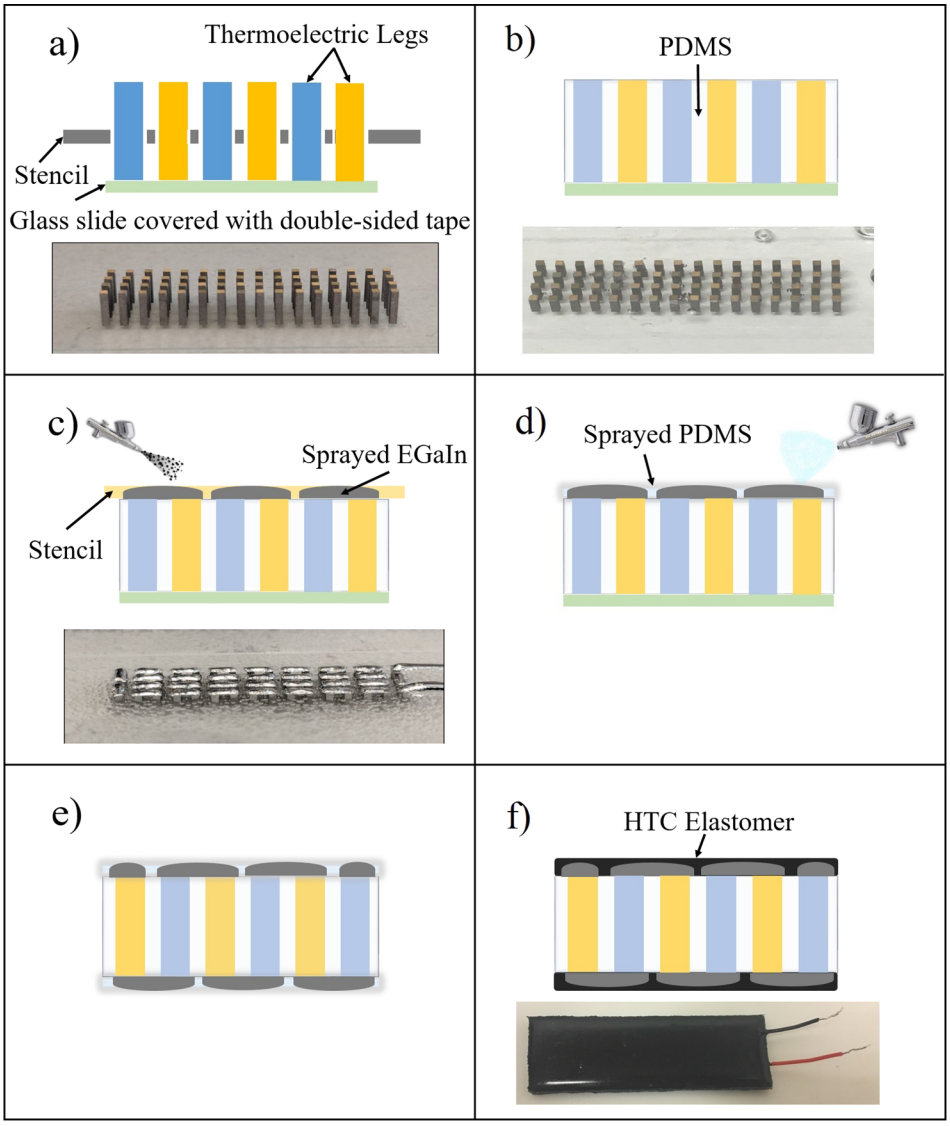


**Fig. 2.** The process flow used in fabrication of flexible thermoelectric generators. (a) The legs are placed through a template; (b) PDMS is poured between the legs, planarized and cured; (c) EGaIn interconnects are sprayed through a hard mask; (d) A thin (~50 μm) layer of PDMS is sprayed as temporary encapsulation; (e) The device is flipped and liquid metal interconnects are sprayed and encapsulated on the backside; (f) Final high thermal conductivity encapsulation elastomer is drop-casted on both sides of the device and cured.

**Table 1**
Properties of thermoelectric legs.

| Parameter | N-type legs | P-type legs |
|---|---|---|
| Electrical Conductivity | 1100 S/cm | 820 S/cm |
| Thermal Conductivity | Unknown | 1.45 W/mK |
| Seebeck Coefficient | −220 μV/K | 220 μV/K |

temperature varied between 20°C and 22°C during the measurements. Each measurement was performed approximately 5 min after placing the TEG on the hotplate. All measurements were repeated three times and the average values were calculated. Finally, the best fabricated TEG was incorporated into a wristband made using Ecoflex™ (a commercially available elastomer). Hook-and-loop fastener strips were also attached to the two ends of the Ecoflex band to fasten the device around the wrist (Fig. 5b). The TEG was tested on the wrist using the same setup as before.

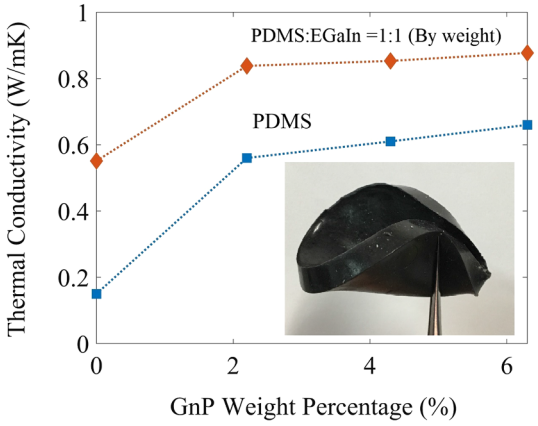


**Fig. 3.** Thermal conductivity of the encapsulation elastomer with and without EGaIn inclusion as a function of the GnP weight percentage. (Inset: A cured sample doped with 50 wt% liquid metal (EGaIn) and 2.2 wt% GnP.)

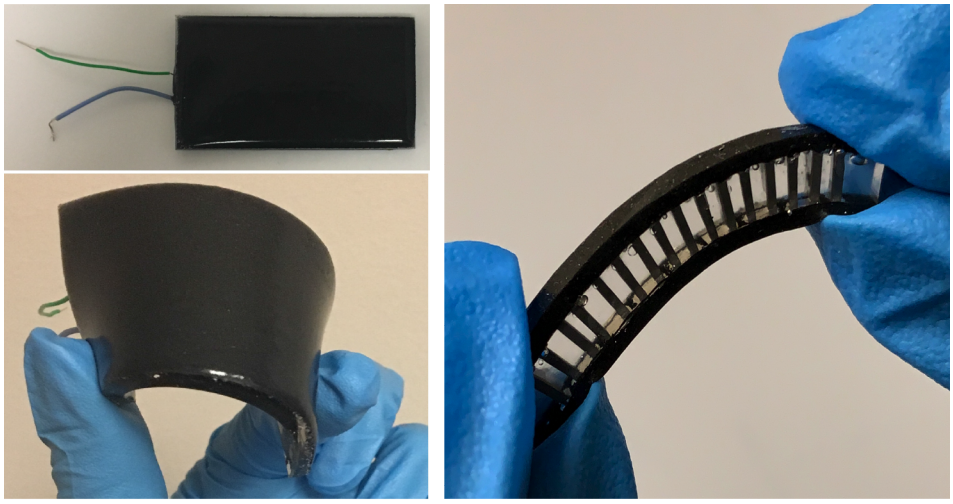

**Fig. 4.** (a) A thermoelectric generator made with high thermal conductivity encapsulation. (b) Cross-sectional image of the device.

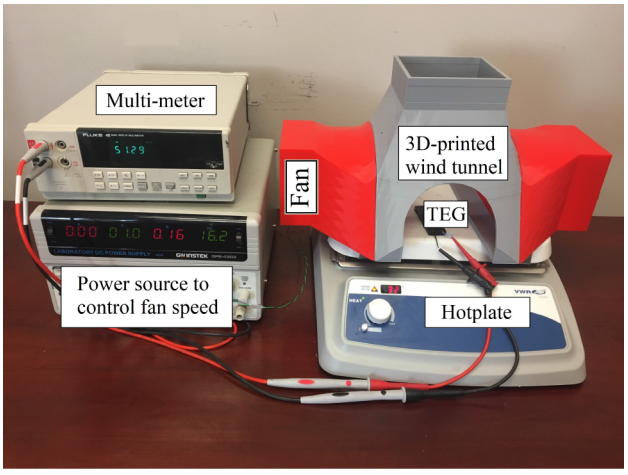


(a)

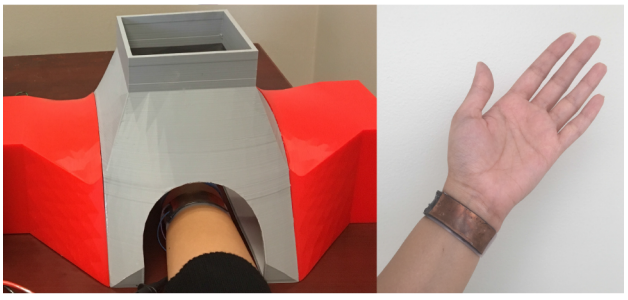

(b)

**Fig. 5.** (a) Setup used to characterize the thermoelectric generators On the hotplate. (b) TEG worn on the wrist inside and outside of the wind tunnel.

## 3. Results

### 3.1. Impact of EGaIn encapsulation on device performance

TEGs were fabricated using either pure PDMS or the HTC elastomer encapsulation to compare the impact of thermal conductivity on device performance. For both materials, two different thicknesses of 300 or 800 μm were used to vary the encapsulation thermal resistance. Fig. 6a shows the open-circuit voltage, $V_{oc}$, for four different TEGs fabricated using the above variations in TEG construction. All four TEGs were fabricated with a fill factor of 20%. We measured $V_{oc}$ as a function of the airflow for velocities ranging from zero (natural convection) to 1.2 m/s (walking speed). We can see that $V_{oc}$ increases significantly as a result of reducing the thickness of the pure PDMS encapsulation from 800 μm to 300 μm, which is expected due to the appreciable reduction of the encapsulation thermal resistance on both sides of the device. Using the thermal conductivity provided for the thermoelectric legs in Table 2, the thermal resistance of a single leg (0.7 mm × 0.7mm × 3mm) can be calculated as 4100 K/W. Using a thermal conductivity of 0.15 W/mK for pure PDMS (Fig. 3), the thermal resistance of a 300 μm thick PDMS layer of the same base area as the legs is 10X larger than that of a single leg. Therefore, an encapsulation layer with such high resistance on either side of the device would be expected to significantly lower the temperature differential, ΔT, across the legs. This observation is supported by the measurements shown in Fig. 6a for devices with the HTC elastomer. For the thinner, 300 μm insulation, $V_{oc}$ is 1.3X higher with the HTC elastomer at an air velocity of 1.2 m/s. It is interesting to note that when the HTC encapsulation thickness increases to 800 μm, we observe only a small drop in $V_{oc}$. This suggests that due to the higher thermal conductivity of the HTC elastomer, the penalty for increasing the encapsulation thickness is much reduced, thus allowing the use of a thicker layer for increased robustness. Nevertheless, in our experience, 300 μm encapsulation was found to be sufficiently thick to achieve a robust encapsulation layer with no sign of EGaIn leakage through the elastomer during regular handling. The measured $V_{oc}$ levels were used to calculate the output power, $P$, assuming a matching load resistance. The output power can be expressed as

$$P = \frac{V_{OC}^2}{4 \times R_{TEG}} \quad (1)$$

where $R_{TEG}$ is the TEG resistance, measured as 6.5 ± 0.5Ω for all our devices fabricated in this study. Fig. 6b shows the power density of the TEGs calculated using the above equation. For an encapsulation thickness of 300 μm, a 1.7X improvement in power density was obtained at 1.2 m/s as a result of replacing PDMS with the HTC elastomer. It is encouraging to note that even with natural convection (i.e., no air flow) the power density is around 10 μm/cm$^2$. At 1.2 m/s, the power density jumps to 45 μW/cm$^2$.

To support the measurements, we used COMSOL Multi-physics software to simulate the temperature gradient across a single thermoelectric leg using the structure shown in Fig. 7a, which closely mimics the fabricated devices. In these simulations, we used an EGaIn

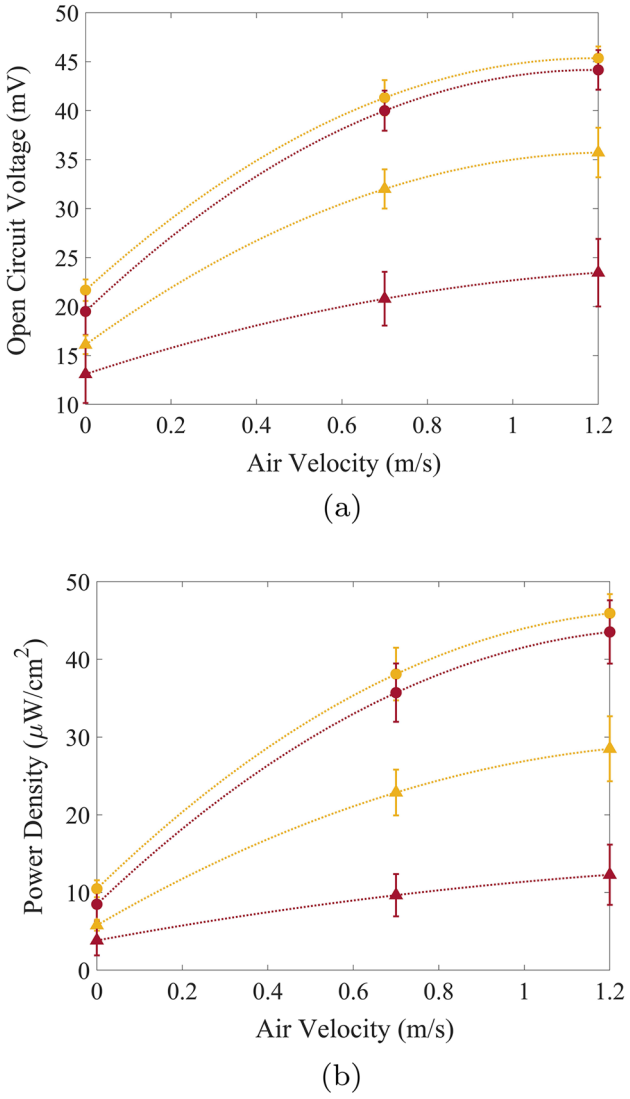


**Fig. 6.** Device performance measured for different encapsulation layers. (a) Measured open-circuit voltage versus air velocity. (b) Calculated power density of thermoelectric generators with 20% fill factor. The numbers in the labels refer to the thickness of the encasing layer. The lines are just used to guide the eye. Decreasing the thickness of PDMS or increasing the thermal conductivity helps improve the power density.

**Table 2**
Parameters used in COMSOL simulation.

| Parameter | Value | Unit |
|---|---|---|
| thermoelectric leg electrical conductivity | 1000 | S/cm |
| thermoelectric leg thermal conductivity | 1.45 | W/mK |
| thermoelectric leg Seebeck coefficient | ± 220 | μV/K |
| EGaIn electrical resistivity | 2.94 | μΩ·cm |
| EGaIn thickness | 200 | μm |
| EGaIn Interconnect width | 750 | μm |
| Filler (PDMS) thermal conductivity | 0.15 | W/mK |
| Heat Transfer Coefficient (Natural Convection) | 5 | $W/m^2 K$ |
| Ambient Temperature | 21 | °C |
| Hot Side Temperature | 32 | °C |

interconnect thickness of 200 μm. The EGaIn encapsulation consists of a 50 μm thick elastomer that conforms to the EGaIn interconnects and a second, thicker planarized elastomer. We varied the thermal conductivity of the second encapsulation layer from 0.1 (below PDMS) to 2 W/mK and its thickness from 100 to 1000 μm covering the range considered to fabricate our devices. The other parameters used in the simulations are listed in Table 2. The simulation results summarized in Fig. 7b, are in close agreement with the measurement results shown in Fig. 6. Clearly, the temperature differential across the leg increases with increasing thermal conductivity of the encapsulation regardless of the encapsulation thickness. The dependence of the temperature differential on the encapsulation thickness is strongest for the lowest thermal conductivity of 0.1 W/mK but it decreases with the increasing thermal conductivity of the elastomer. At the highest thermal conductivity of 2 W/mK, the thickness dependence is negligibly small, which means that a thicker elastomer can be used without appreciable degradation in device performance. The simulation results suggest that the thermal conductivity of 0.85 W/mK used in this study brings us fairly close to the best performance possible with the proposed device architecture.

### 3.2. Impact of fill factor on device performance

Conventional rigid TEGs typically have air between their legs. With a thermal conductivity of 0.025 W/mK [55,1], air is approximately 60X less conductive than bismuth-based chalcogenides used in TEGs optimized for room temperature applications. Thus, in rigid TEGs, almost the entire heat provided by the source is forced to flow through the legs. In a flexible TEG, typically, a flexible material with a considerably higher thermal conductivity fills the space between the legs. For example, PDMS used in this study is approximately 6X more conductive than air, thus providing an undesirable conductive path for heat. To study the impact of the fill factor on the performance of our flexible TEGs, we fabricated modules with three different fill factors of 5, 13 and 20%. The corresponding TEG areas were 1.6, 3.0, and 6.4 $cm^2$ respectively. The EGaIn interconnects were encapsulated with a 300 μm thick PDMS or HTC elastomer layer. The $V_{oc}$ levels measured from TEGs at different air velocities and the corresponding power density figures are plotted in Fig. 8. We can see that for the TEGs with PDMS encapsulation, $V_{oc}$ appears to increase slightly with the fill factor. This behavior may be attributed to the reduction in the area occupied by the filler elastomer at higher fill factors. Interestingly however, with HTC encapsulation, we do not observe a discernable dependence on fill factor. We speculate that the heat spreading provided by the HTC encapsulation somewhat compensates for the loss by increasing the area available for heat collection/rejection around each leg.

### 3.3. Impact of copper heat spreader on device performance

A rigid TEG relies on its thermally conductive “headers“ to spread heat laterally for effective heat collection on the hot side and effective heat rejection on the cold side. While the HTC elastomer provides some contribution to the lateral heat spreading, its resistivity is still high compared to the typical header materials used in rigid TEGs. The thermal sheet resistance of a 300 μm thick HTC elastomer can be calculated as 3900 K/W per square. In contrast, the thermal sheet resistance of a 1 μm thick copper layer is approximately 2600 K/W per square assuming a copper thermal conductivity of 385 W/mK [56]. Therefore, a thin copper layer has the potential to improve the lateral heat spreading, further reducing the parasitic resistance on either side of the device. Fig. 9 shows the simulated $\Delta T$ across a single central leg of a 64-leg TEG as a function of the Cu spreader thickness. For these simulations, we added a thin Cu spreader on the cold side of the 3-D structure shown in Fig. 7. We assumed natural convection (i.e. zero airflow) as the primary heat rejection mechanism. We can see that the simulated $\Delta T$ increases with the Cu thickness providing a $V_{oc}$ improvement on the order of ~30% before leveling off at around 8 μm, where, the thermal sheet resistance of the spreader is 12X lower than that of the HTC elastomer. Therefore, we anticipate a significant contribution from such a layer to the lateral heat spreading. To verify, we fabricated flexible TEGs with 8 μm thick Cu heat spreaders. A typical module is shown in Fig. 10. The spreader was deposited only on one

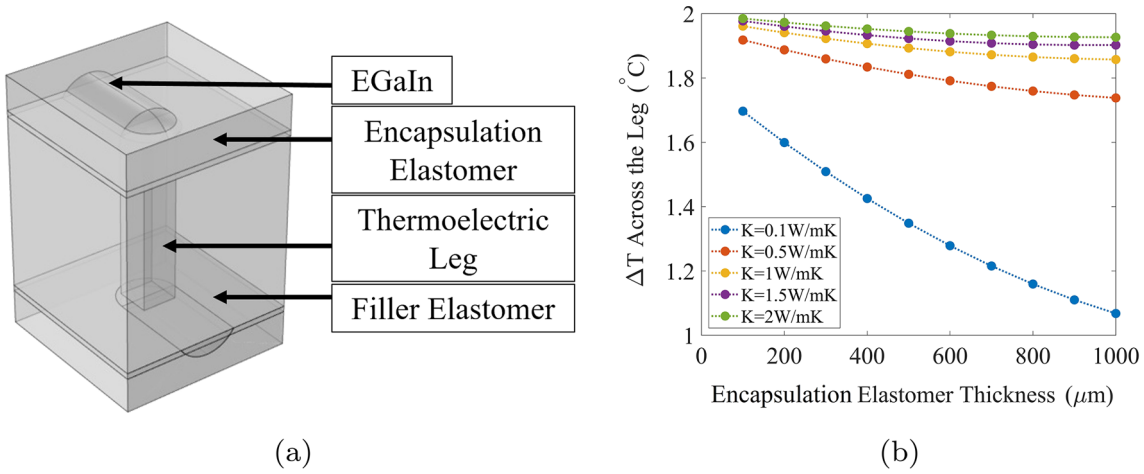


**Fig. 7.** (a) The 3-D structure used in COMSOL simulations; (b) Simulated temperature drop across a single thermoelectric leg as a function encapsulating elastomer thickness for different elastomer thermal conductivities.

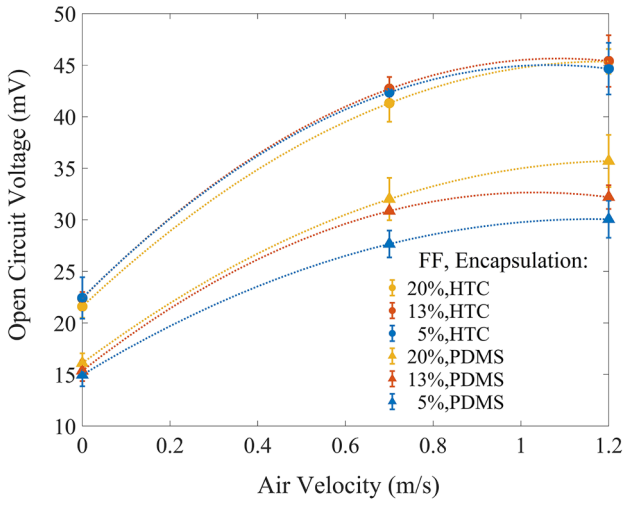


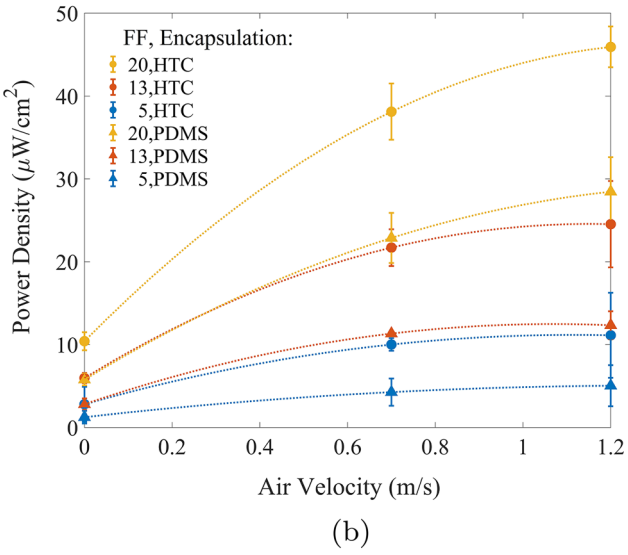


**Fig. 8.** (a) Open-circuit voltage measured for thermoelectric generators made with high thermal conductivity and PDMS encapsulation with different fill factors (FF). (b) Corresponding power density for those devices. The lines are used just to guide the eye.

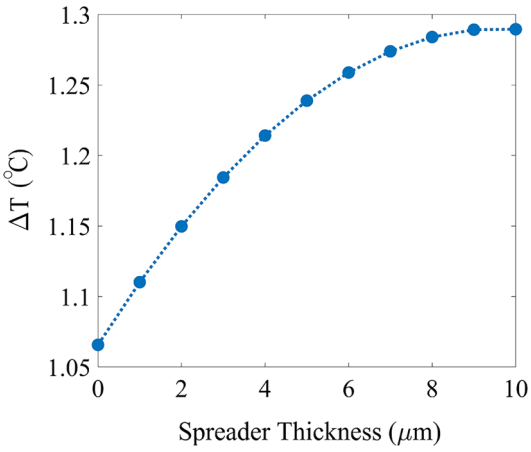


**Fig. 9.** Modeled ΔT across a single leg in a 64 leg thermoelectric generator plotted as a function of the copper spreader thickness.

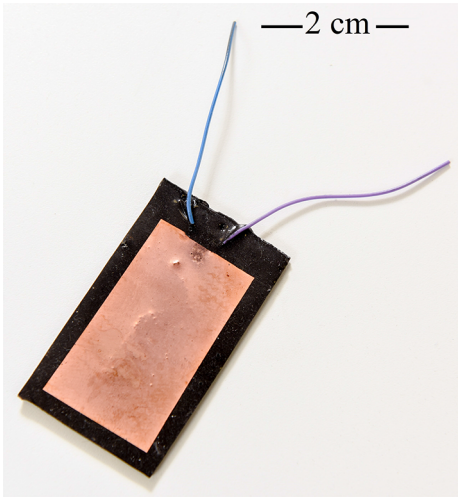


**Fig. 10.** Thermoelectric generator with an electroplated copper spreader layer on top of HTC elastomer.

side of the TEG. Fig. 11 shows measured $V_{oc}$ levels with and without the Cu spreader on the cold side of the flexible TEG. As shown, higher $V_{oc}$ levels are obtained with the Cu spreaders at all air velocities regardless of the encapsulation material. Interestingly however, with either HTC

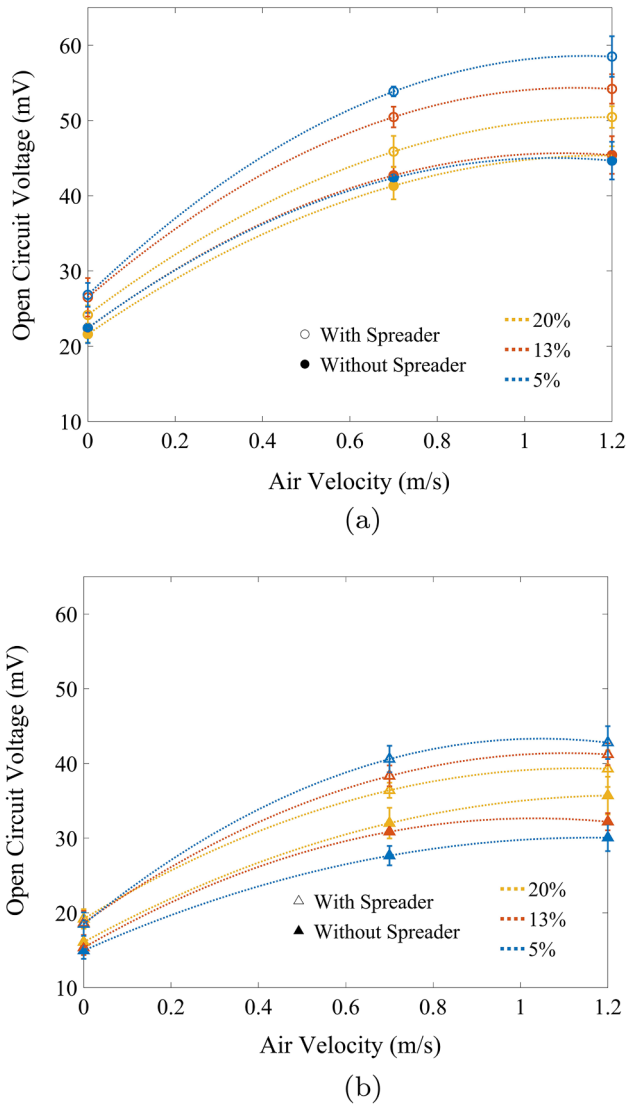


**Fig. 11.** (a) Open-circuit voltage measured for thermoelectric generators made using high thermal conductivity encapsulation (with different fill factors of 5, 13, 20%) with and without a copper spreader layer. (b) Open-circuit voltage measured for thermoelectric generators with PDMS encapsulation with and without copper spreader. The lines are used just to guide the eye.

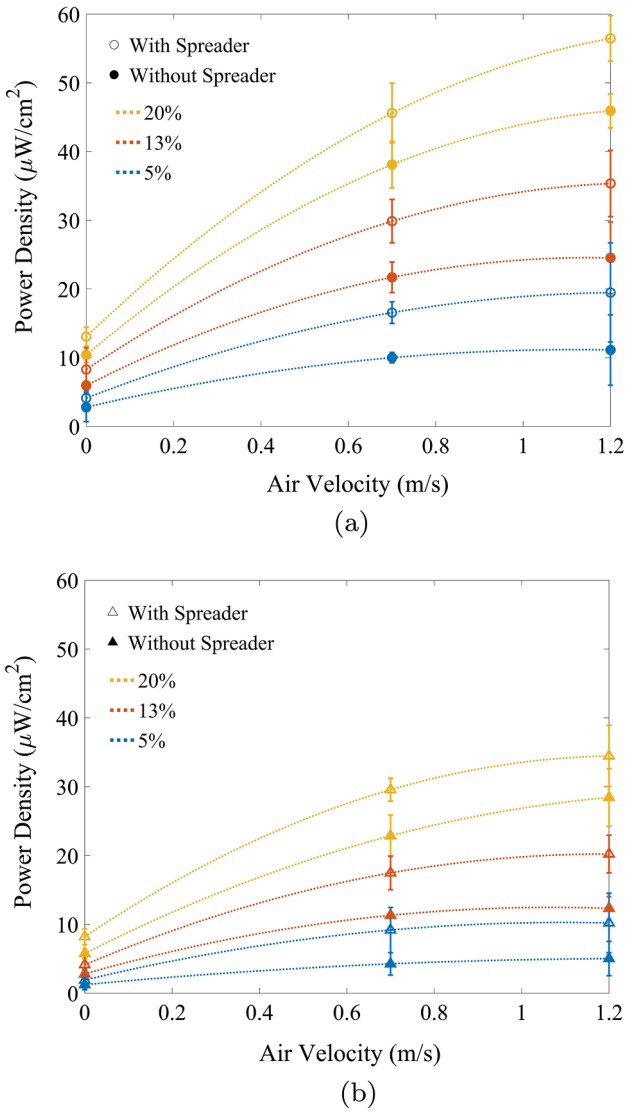


**Fig. 12.** (a) Power density for devices fabricated using high thermal conductivity encapsulation (with different fill factors of 5, 13, 20%) with and without copper spreader. (b) Power density for devices fabricated using PDMS EGaIn encapsulation with and without copper spreader. The lines are used just to guide the eye.

or PDMS encapsulation, larger $V_{oc}$ levels are obtained at lower fill factors. This result is consistent with the observations of Suarez et al. [52], who argued that increasing the module area by reducing the leg density would reduce the thermal contact resistances at the TEG/skin and TEG/air interfaces thereby increasing the ratio of the TEG thermal resistance to the total resistance, which ultimately determines the $\Delta T$ across the legs. As shown in Fig. 11b, with PDMS encapsulation, this effect is strong enough to reverse the dependence of $V_{oc}$ on the fill factor.

Fig. 12 shows the power density figures calculated using the measured $V_{oc}$ levels. We can see that the power density improves significantly with the addition of the Cu spreader. Furthermore, the dependence on fill factor is reversed yielding higher power density figures at higher fill factors. It is evident that the HTC elastomer and the Cu spreader are working in conjunction to improve the device performance. Comparison of the power levels of devices fabricated with a fill factor of 20% reveals that the copper spreader provides a 1.2X-1.3X improvement in power density at an air velocity of 1.2 m/s. We note that, unless this 20–30% improvement is essential for a specific application, the spreader may be omitted considering the additional complexity of electroplating Cu on the elastomer. A simpler approach might be an integrated flexible heatsink or larger device area.

### *3.4. Device flexibility and impact of mechanical bending on device performance*

Much of the earlier work on flexible electronics focused on the variations that occurred in the electrical properties of devices and circuits upon flexing them [57–62]. Flexible TEGs proposed to date by various groups around the world employed different device architectures and a variety of flexible and stretchable materials. Therefore, there is a need to develop a standard procedure to benchmark the flexibility of different TEGs. In this work, we have made an attempt to develop a standard procedure to compare flexibility of different TEG modules. In this study, we used a force gauge to measure the force needed to bend a flexible TEG to a known diameter. Fig. 13a shows the set-up. The bending diameter used in our measurements was 9 cm. We applied this method to TEGs with different fill factors since device flexibility is naturally affected by the spacing between the rigid legs. The measurements were also repeated for control samples consisting of either pure PDMS or the HTC/PDMS/

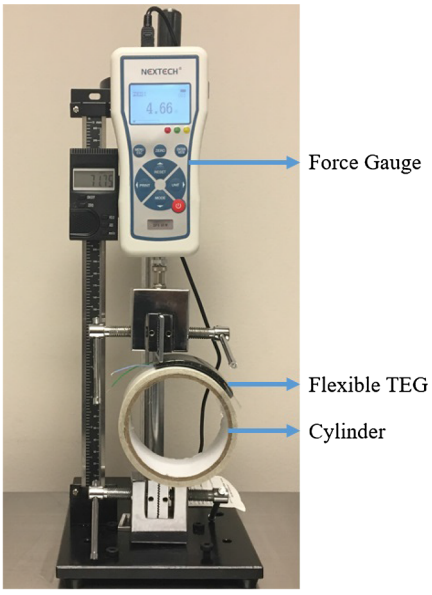


(a)

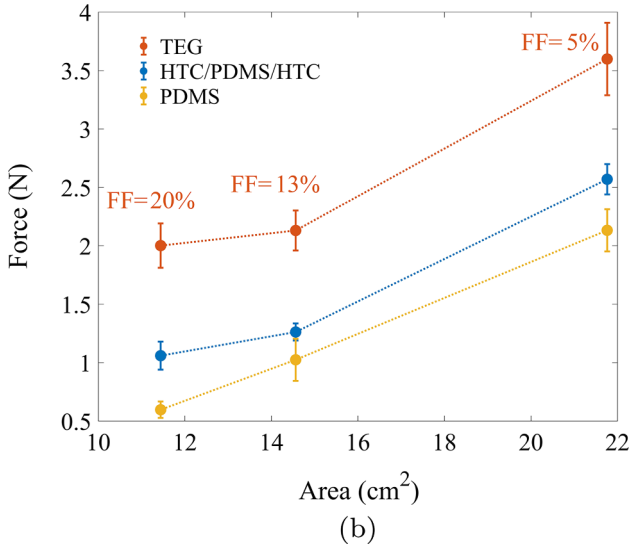


(b)

**Fig. 13.** (a) Setup used to measure force required to bend the devices around a cylinder. (b) Force required to keep the thermoelectric generators and control samples bent around a cylinder. (FF: fill factor).

HTC stack (total thickness of 3.7 mm) used in our devices without the rigid thermoelectric legs. We note that since all TEGs have 64 legs, different fill factors correspond to different TEG and control sample areas. The fill factors of 5, 13 and 20% yield TEG areas of 21.76, 14.56, and 11.44 $cm^2$ respectively. The measured force is plotted in Fig. 13b for different TEGs and control samples. As expected, the force needed to bend the samples increases with the sample area for all three cases. We note that the bending force is slightly higher for the HTC/PDMS/HTC stack, which is expected due to the higher Young's modulus of the HTC elastomer [54]. As expected, the bending force further increases with incorporation of the rigid thermoelectric legs. It is interesting to note that this increase is independent of the fill factor or the device area. We note that the flexibility of these TEGs is largely dependent on the flexibility of PDMS used as the base elastomer in this study. There is a potential to appreciably increase the flexibility of these devices by employing newer elastomers such as Ecoflex™ and Dragonskin with lower Young's moduli [63–65].

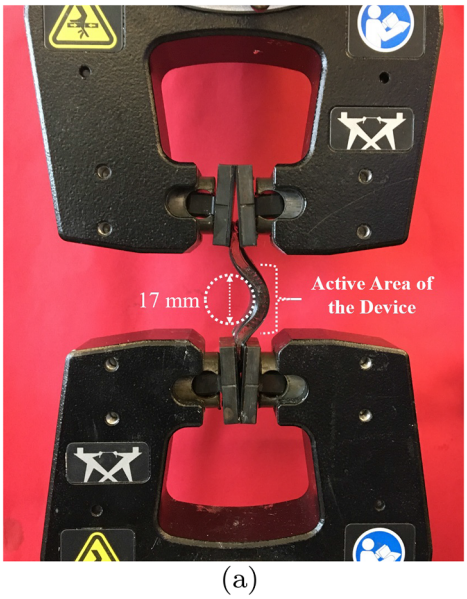


(a)

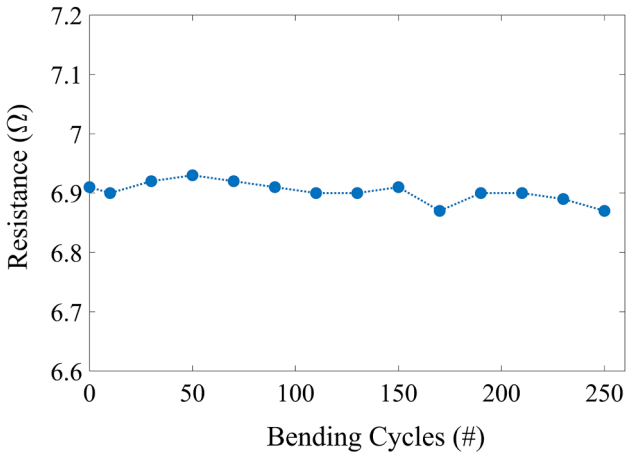


(b)

**Fig. 14.** (a) Setup used to measure the electrical resistance of a thermoelectric generator with a fill factor of 20% at a bending radius of 17 mm. (b) AC electrical resistance of the device as a function of the number of bending cycles. The resistance measurement was repeated every 20 cycles.

To investigate the impact of bending on total TEG electrical resistance and the reliability of interconnects upon repeated bending cycles, we used the tensile testing system (Instron™ 5943) shown in Fig. 14a. The system was programmed to repeatedly flex the TEG to a bending diameter of 17 mm at 0.5 cycles/second for 250 bending cycles. The AC electrical resistance was measured after each 20 cycles by a DX 4090 Z-Meter manufactured by TEC-Microsystems. The measured electrical resistance is shown in Fig. 14b as a function of the number of bending cycles. As shown, the electrical resistance of the TEG remains constant within ± 0.5% during the entire measurement with no signs of failure after 250 bending cycles.

To evaluate the impact of mechanical bending on TEG performance, we measured the open-circuit voltage of flexible TEGs mounted on heated metal with different diameters. A flexible heater coil was wrapped around the pipes and powered to reach a steady temperature of 32°C immediately under the flexible TEG. The set-up is shown in Fig. 15. We used metal pipes with three different diameters of 2.54 cm, 5.08 cm, and 7.62 cm. The measurements were performed using the same procedure we used for the hot-plate measurements. The measured open circuit voltage and the corresponding power density are shown in

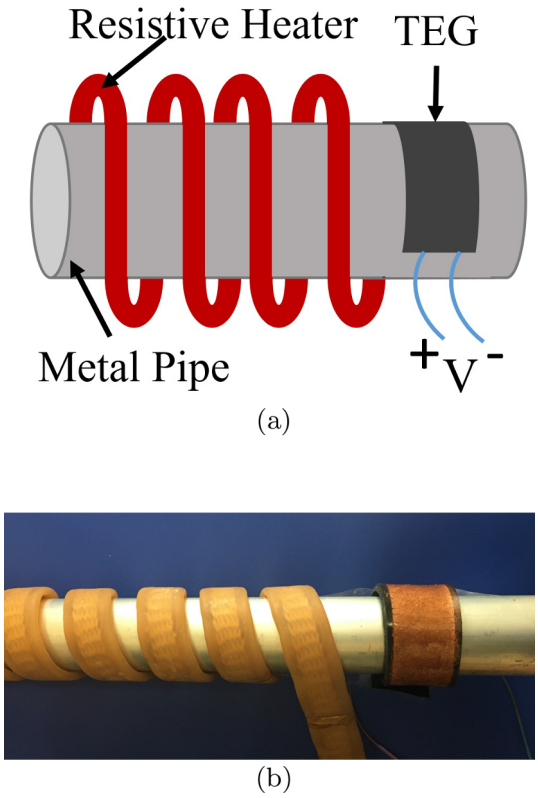


**Fig. 15.** (a) Schematic, and (b) a picture of the setup used to measure the thermoelectric generators around different pipes.

Fig. 16a and b respectively. It is important to note that the AC electrical resistance used to calculate the power density levels did not change with bending. $V_{oc}$ and power density levels measured on a hotplate are also included in the plots. The measurements reveal a small but measurable difference in TEG performance with bending. This behavior may be attributed to different factors including the thickening of the bottom encapsulation layer under compression, which would increase the parasitic thermal resistance between the legs and the human body. With air flow, the thermal resistance between the TEG and the ambient is also expected to change due to the smaller TEG area exposed to air flow with smaller pipe diameters. In conclusion, the measurements suggest that the generated voltage decreases with decreasing bending diameter. On the pipe with the smallest diameter of 1 in., the drop in $V_{oc}$ is close to 20%.

### 3.5. TEG performance on human wrist

Since the ultimate goal of this work is to develop high performance flexible TEGs for wearable applications, we have used our best performing TEG (with 300 μm thick HTC elastomer and copper spreader, fill factor = 20%) on the wrist as shown in Fig. 17a. The open-circuit voltage, $V_{oc}$, and the output power density of the TEG are shown in Fig. 17b and c respectively. We can see that the behavior of the TEG at different air velocities (generated by the fan) is similar to that obtained on the hotplate. We can see that $V_{oc}$ first increases with increasing air velocity but levels off after a certain point. During these measurements, the measured skin temperature was around 30–31°C, which is lower than the standard hot-plate temperature of 32°C used for the other measurements. We note that, the airflow over the skin can potentially reduce the skin temperature [66]. The measured output power produced by the TEG on the wrist at an air velocity of 1.2 m/s shows can reach 35 μW/cm$^2$, which is quite promising. Therefore, a flexible TEG with an area of 100 cm$^2$ can provide a power level on the order of 1 mW, which is more than sufficient to power low-power sensors and

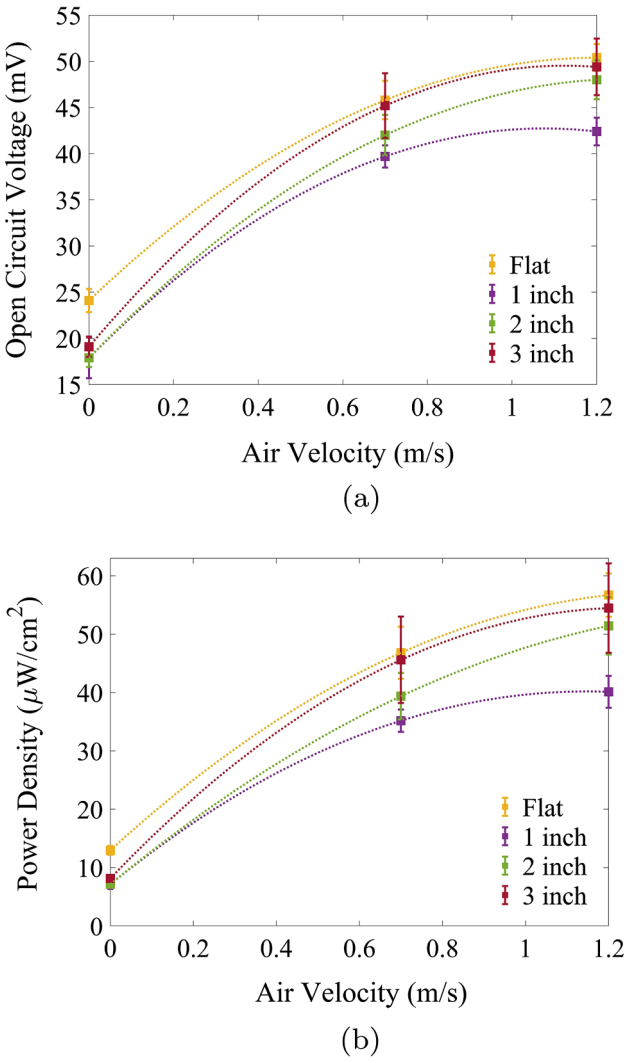


**Fig. 16.** (a) Open-circuit voltage measured for the thermoelectric generator made with high thermal conductivity encapsulation and copper spreader with a fill factor of 20%. (b) Corresponding power density for the device. The lines are used just to guide the eye.

electronics. This result also suggests that flexible TEGs with liquid metal interconnects have the potential to rival their rigid counterparts for future self-powered wearables [67–69].

Table 3 summarizes the power density levels generated by several of the best flexible TEGs reported to date. TEGs presented in this table were characterized on a hot surface (other than the human body) relying on natural convection to reject heat from the cold side.

Table 4 compares several of the best flexible TEGs tested on the human body with natural convection. The table reports the ambient temperature used for the measurements. A cooler ambient implies a larger ΔT and higher performance. We note that the best performing devices employ rigid thermoelectric legs. The TEG reported in this study shows the highest power density of 5.2 μW/cm$^2$ at an ambient temperature of 21°C.

## 4. Conclusions

This paper reports high performance flexible thermoelectric generators (TEGs) with rigid P- and N-type bismuth chalcogenide thermoelectric legs connected in series with low-resistivity, self-healing, stretchable liquid metal interconnects. The focus of this report is the thermal conductivity of the material used to encapsulate the liquid

(a)

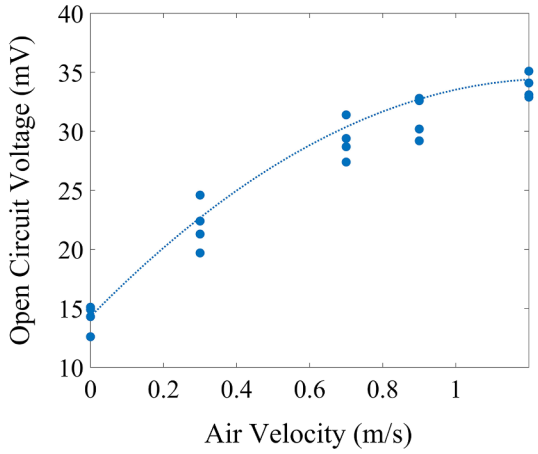


(b)

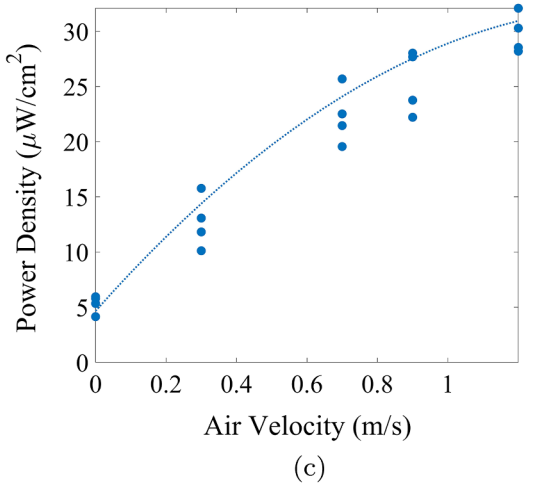


(c)

**Fig. 17.** (a) Image of the thermoelectric generator worn on the wrist. (b) Open-circuit voltage measured on the wrist for the thermoelectric generator made with high thermal conductivity encapsulation and copper spreader with a fill factor of 20%. (c) Corresponding power density for the device. The lines are used just to guide the eye.

metal interconnects. In this work, we demonstrated TEGs fabricated using a novel stretchable, high thermal conductivity elastomer consisting of polydimethylsiloxane (PDMS) with graphene nano-platelets/EGaIn inclusions. This material can provide a thermal conductivity of 0.85 W/mK corresponding to a 5.6X improvement over that of pure PDMS. Through experimental work and modeling, we show that a thermal conductivity close to 1 W/mK is needed to minimize the impact of the encapsulation resistance on device performance. We also show that the device performance can be further improved by adding a thin copper heat spreader. The resulting TEGs worn on the wrist produce power density levels approaching 35 μW/cm$^2$ at air velocities corresponding to average walking speed. These performance figures make this devices one of the best performing wearable flexible TEGs reported to date. More importantly, the results suggest that our approach is capable of producing flexible, large-area TEGs that have the potential to rival the performance of rigid TEGs in wearable applications. This unique approach eliminates the need to develop new thermoelectric materials to create flexible TEGs. Furthermore, with a fabrication procedure that closely mimics rigid TEG manufacturing, the approach offers a flexible TEG with a low cost-of-ownership, especially for existing rigid TEG manufacturers.

**Table 3**
Power density of different flexible TEGs characterized on a hot-plate or similar heated surface relying on natural convection on the cold side.

| Fabrication method | $\Delta T$ (°C) | Power density (μW/cm$^2$) | Reference |
|---|---|---|---|
| Electrodeposition | 22 | 3 | [2] |
| Screen Printing | 20 | $41 \times 10^{-3}$ | [36] |
| Bulk | 5 | 0.3 | [7] |
| Bulk | 8.9 | 2.28 | [6] |
| Bulk | 11 | 12 | This work |

**Table 4**
Power density of different flexible TEGs characterized on the human body with natural convection.

| Fabrication method | Ambient temperature (°C) | Power density (μW/cm$^2$) | Reference |
|---|---|---|---|
| Dispenser printing | 13 | $84 \times 10^{-3}$ | [70] |
| Wet spinning of CNT | 24 | $0.125 \times 10^{-3}$ | [35] |
| Chemical Exfoliating | 25 | $0.73 \times 10^{-3}$ | [27] |
| Screen Printing | 17 | 0.73 | [23] |
| Bulk | 25 | 0.526 | [7] |
| Bulk | 5 | 2.5 | [8] |
| Bulk | 21 | 5.2 | This work |

## CRediT authorship contribution statement

**Yasaman Sargolzaeiaval:** Conceptualization, Methodology, Validation, Formal analysis, Investigation, Writing - original draft, Writing - review & editing, Visualization. **Viswanath Padmanabhan Ramesh:** Conceptualization, Methodology, Visualization, Investigation. **Taylor V. Neumann:** Investigation, Validation, Visualization. **Veena Misra:** Resources, Visualization, Supervision, Project administration. **Daryoosh Vashaee:** Resources, Supervision. **Michael D. Dickey:** Investigation, Resources, Writing - review & editing, Supervision, Project administration. **Mehmet C. Öztürk:** Conceptualization, Methodology, Investigation, Resources, Writing - review & editing, Visualization, Supervision, Project administration, Funding acquisition.

## Declaration of Competing Interest

The authors declare that they have no known competing financial interests or personal relationships that could have appeared to influence the work reported in this paper.

## Acknowledgements

This work was supported by the Advanced Self-Powered Systems of Integrated Sensors and Technologies (ASSIST), a Nano-Systems

Engineering Research Center funded by National Science Foundation (EEC1160483). The authors would like to thank Abhishek Malhotra for measuring the properties of the thermoelectric legs, Nicole Hedges and Marcio Cerullo of the NCSU nanofabrication facility (NNF) for their help in the cleanroom.

## References


[1] Siddique ARM, Mahmud S, Van Heyst B. A review of the state of the science on wearable thermoelectric power generators (tegs) and their existing challenges. Renew Sustain Energy Rev 2017;73:730–44.
[2] Huu TN, Van TN, Takahito O. Flexible thermoelectric power generator with y-type structure using electrochemical deposition process. Appl Energy 2018;210:467–76.
[3] Kim SJ, Lee HE, Choi H, Kim Y, We JH, Shin JS, et al. High-performance flexible thermoelectric power generator using laser multiscanning lift-off process. ACS Nano 2016;10(12):10851–7.
[4] Eom Y, Wijethunge D, Park H, Park SH, Kim W. Flexible thermoelectric power generation system based on rigid inorganic bulk materials. Appl Energy 2017;206:649–56.
[5] Park H, Lee D, Kim D, Cho H, Eom Y, Hwang J, et al. High power output from body heat harvesting based on flexible thermoelectric system with low thermal contact resistance. J Phys D Appl Phys 2018;51(36):365501.
[6] Kim CS, Lee GS, Choi H, Kim YJ, Yang HM, Lim SH, et al. Structural design of a flexible thermoelectric power generator for wearable applications. Appl Energy 2018;214:131–8.
[7] Wang Y, Shi Y, Mei D, Chen Z. Wearable thermoelectric generator to harvest body heat for powering a miniaturized accelerometer. Appl Energy 2018;215:690–8.
[8] Suarez F, Parekh DP, Ladd C, Vashaee D, Dickey MD, Öztürk MC. Flexible thermoelectric generator using bulk legs and liquid metal interconnects for wearable electronics. Appl Energy 2017;202:736–45.
[9] Jeong SH, Cruz FJ, Chen S, Gravier L, Liu J, Wu Z, et al. Stretchable thermoelectric generators metallized with liquid alloy. ACS Appl Mater Interfaces 2017;9(18):15791–7.
[10] Choi H, Kim YJ, Kim CS, Yang HM, Oh M-W, Cho BJ. Enhancement of reproducibility and reliability in a high-performance flexible thermoelectric generator using screen-printed materials. Nano Energy 2018;46:39–44.
[11] Saha C, O'donnell T, Wang N, McCloskey P. Electromagnetic generator for harvesting energy from human motion. Sens Actuators A: Phys 2008;147(1):248–53.
[12] Mitcheson PD, Yeatman EM, Rao GK, Holmes AS, Green TC. Energy harvesting from human and machine motion for wireless electronic devices. Proc IEEE 2008;96(9):1457–86.
[13] Liu R, Kuang X, Deng J, Wang Y-C, Wang AC, Ding W, et al. Shape memory polymers for body motion energy harvesting and self-powered mechanosensing. Adv Mater 2018;30(8):1705195.
[14] Proto A, Penhaker M, Bibbo D, Vala D, Conforto S, Schmid M. Measurements of generated energy/electrical quantities from locomotion activities using piezoelectric wearable sensors for body motion energy harvesting. Sensors 2016;16(4):524.
[15] Dagdeviren C, Yang BD, Su Y, Tran PL, Joe P, Anderson E, et al. Conformal piezoelectric energy harvesting and storage from motions of the heart, lung, and diaphragm. Proc Natl Acad Sci 2014;111(5):1927–32.
[16] Romero E, Warrington RO, Neuman MR. Body motion for powering biomedical devices. In: 2009 annual international conference of the IEEE engineering in medicine and biology society, IEEE; 2009. p. 2752–5.
[17] Nasir AA, Zhou X, Durrani S, Kennedy RA. Relaying protocols for wireless energy harvesting and information processing. IEEE Trans Wireless Commun 2013;12(7):3622–36.
[18] Ulukus S, Yener A, Erkip E, Simeone O, Zorzi M, Grover P, et al. Energy harvesting wireless communications: a review of recent advances. IEEE J Sel Areas Commun 2015;33(3):360–81.
[19] Visser HJ, Vullers RJ. Rf energy harvesting and transport for wireless sensor network applications: principles and requirements. Proc IEEE 2013;101(6):1410–23.
[20] Lee S, Zhang R, Huang K. Opportunistic wireless energy harvesting in cognitive radio networks. IEEE Trans Wireless Commun 2013;12(9):4788–99.
[21] Kamalinejad P, Mahapatra C, Sheng Z, Mirabbasi S, Leung VC, Guan YL. Wireless energy harvesting for the internet of things. IEEE Commun Mag 2015;53(6):102–8.
[22] Nozariasbmarz A, Collins H, Dsouza K, Polash MH, Hosseini M, Hyland M, et al. Review of wearable thermoelectric energy harvesting: From body temperature to electronic systems. Appl Energy 2019;114069.
[23] Kim SJ, We JH, Cho BJ. A wearable thermoelectric generator fabricated on a glass fabric. Energy Environ Sci 2014;7(6):1959–65.
[24] Toshima N. Recent progress of organic and hybrid thermoelectric materials. Synth Met 2017;225:3–21.
[25] Chen G, Xu W, Zhu D. Recent advances in organic polymer thermoelectric composites. J Mater Chem C 2017;5(18):4350–60.
[26] Yang P, Liu K, Chen Q, Mo X, Zhou Y, Li S, et al. Wearable thermocells based on gel electrolytes for the utilization of body heat. Angew Chem Int Ed 2016;55(39):12050–3.
[27] Oh JY, Lee JH, Han SW, Chae SS, Bae EJ, Kang YH, et al. Chemically exfoliated transition metal dichalcogenide nanosheet-based wearable thermoelectric generators. Energy Environ Sci 2016;9(5):1696–705.
[28] Du Y, Cai K, Chen S, Wang H, Shen SZ, Donelson R, et al. Thermoelectric fabrics: toward power generating clothing. Sci Rep 2015;5:6411.
[29] Itoigawa K, Ueno H, Shiozaki M, Toriyama T, Sugiyama S. Fabrication of flexible thermopile generator. J Micromech Microeng 2005;15(9):S233.
[30] Shiozaki M, Sugiyama S, Watanabe N, Ueno H, Itoigawa K. Flexible thin-film bite thermopile for room temperature power generation. In: 19th IEEE international conference on micro electro mechanical systems, IEEE; 2006. p. 946–9.
[31] Sevilla GAT, Inayat SB, Rojas JP, Hussain AM, Hussain MM. Flexible and semi-transparent thermoelectric energy harvesters from low cost bulk silicon (100). Small 2013;9(23):3916–21.
[32] Weber J, Potje-Kamloth K, Haase F, Detemple P, Völklein F, Doll T. Coin-size coiled-up polymer foil thermoelectric power generator for wearable electronics. Sens Actuators, A 2006;132(1):325–30.
[33] Glatz W, Muntwyler S, Hierold C. Optimization and fabrication of thick flexible polymer based micro thermoelectric generator. Sens Actuators, A 2006;132(1):337–45.
[34] Glatz W, Schwyter E, Durrer L, Hierold C. bi2te3-based flexible micro thermoelectric generator with optimized design. J Microelectromech Syst 2009;18(3):763–72.
[35] Ito M, Koizumi T, Kojima H, Saito T, Nakamura M. From materials to device design of a thermoelectric fabric for wearable energy harvesters. J Mater Chem A 2017;5(24):12068–72.
[36] Cao Z, Koukharenko E, Tudor M, Torah R, Beeby S. Screen printed flexible bi2te3-sb2te3 based thermoelectric generator. Journal of physics: conference series, vol. 476. IOP Publishing; 2013. p. 012031.
[37] Iezzi B, Ankireddy K, Twiddy J, Losego MD, Jur JS. Printed, metallic thermoelectric generators integrated with pipe insulation for powering wireless sensors. Appl Energy 2017;208:758–65.
[38] Wang L, Zhang Z, Geng L, Yuan T, Liu Y, Guo J, et al. Solution-printable fullerene/tis 2 organic/inorganic hybrids for high-performance flexible n-type thermoelectrics. Energy Environ Sci 2018;11(5):1307–17.
[39] Hewitt CA, Kaiser AB, Roth S, Craps M, Czerw R, Carroll DL. Multilayered carbon nanotube/polymer composite based thermoelectric fabrics. Nano Lett 2012;12(3):1307–10.
[40] Lu Z, Zhang H, Mao C, Li CM. Silk fabric-based wearable thermoelectric generator for energy harvesting from the human body. Appl Energy 2016;164:57–63.
[41] Lee JA, Aliev AE, Bykova JS, de Andrade MJ, Kim D, Sim HJ, et al. Woven-yarn thermoelectric textiles. Adv Mater 2016;28(25):5038–44.
[42] Morata A, Pacios M, Gadea G, Flox C, Cadavid D, Cabot A, et al. Large-area and adaptable electrospun silicon-based thermoelectric nanomaterials with high energy conversion efficiencies. Nat Commun 2018;9(1):4759.
[43] Ghafouri N, Kim H, Atashbar MZ, Najafi K. A micro thermoelectric energy scavenger for a hybrid insect. SENSORS, 2008 IEEE. IEEE; 2008. p. 1249–52.
[44] Liu H, Wang Y, Mei D, Shi Y, Chen Z. Design of a wearable thermoelectric generator for harvesting human body energy. Wearable sensors and robots. Springer; 2017. p. 55–66.
[45] Ozturk M, Dickey MD, Ladd C, Parekh DP, Ramesh VP, Suarez F. Flexible thermoelectric generator and methods of manufacturing, uS Patent 10,431,726 (Oct. 1 2019).
[46] Chen B, Kruse M, Xu B, Tutika R, Zheng W, Bartlett MD, et al. Flexible thermoelectric generators with inkjet-printed bismuth telluride nanowires and liquid metal contacts. Nanoscale 2019;11(12):5222–30.
[47] Zrnic D, Swatik D. On the resistivity and surface tension of the eutectic alloy of gallium and indium. J Less Common Metals 1969;18(1):67–8.
[48] Dickey MD. Stretchable and soft electronics using liquid metals. Adv Mater 2017;29(27):1606425.
[49] Chiechi RC, Weiss EA, Dickey MD, Whitesides GM. Eutectic gallium–indium (egain): a moldable liquid metal for electrical characterization of self-assembled monolayers. Angew Chem Int Ed 2008;47(1):142–4.
[50] Yang J, Watson A. An assessment of phase diagram and thermodynamic properties of the gallium-1ndium-antimony system. Calphad 1994;18(2):165–75.
[51] Ayyad A, Freyland W. Wetting transition in liquid ga–bi alloys: light scattering study of surface energy and entropy. Surf Sci 2002;506(1–2):1–11.
[52] Suarez F, Nozariasbmarz A, Vashaee D, Öztürk MC. Designing thermoelectric generators for self-powered wearable electronics. Energy Environ Sci 2016;9(6):2099–113.
[53] Jeong SH, Chen S, Huo J, Gamstedt EK, Liu J, Zhang S-L, et al. Mechanically stretchable and electrically insulating thermal elastomer composite by liquid alloy droplet embedment. Sci Rep 2015;5:18257.
[54] Sargolzaeiaval Y, Ramesh VP, Neumann TV, Miles R, Dickey MD, Öztürk MC. High thermal conductivity silicone elastomer doped with graphene nanoplatelets and eutectic gain liquid metal alloy. ECS J Solid State Sci Technol 2019;8(6):P357–62.
[55] Lemmon EW, Jacobsen R. Viscosity and thermal conductivity equations for nitrogen, oxygen, argon, and air. Int J Thermophys 2004;25(1):21–69.
[56] Nath P, Chopra K. Thermal conductivity of copper films. Thin Solid Films 1974;20(1):53–62.
[57] Kim D-H, Viventi J, Amsden JJ, Xiao J, Vigeland L, Kim Y-S, et al. Dissolvable films of silk fibroin for ultrathin conformal bio-integrated electronics. Nat Mater 2010;9(6):511.
[58] Viventi J, Kim D-H, Moss JD, Kim Y-S, Blanco JA, Annetta N, et al. A conformal, bio-interfaced class of silicon electronics for mapping cardiac electrophysiology. Sci Transl Med 2010;2(24). 24ra22–24ra22.
[59] Ma Y, Jang K-I, Wang L, Jung HN, Kwak JW, Xue Y, et al. Design of strain-limiting substrate materials for stretchable and flexible electronics. Adv Funct Mater 2016;26(29):5345–51.
[60] Chang I, Park T, Lee J, Lee HB, Ko SH, Cha SW. Flexible fuel cell using stiffness-controlled endplate. Int J Hydrogen Energy 2016;41(14):6013–9.
[61] Gao Z, Wien R, Ebrahim T, Flexible display designed for minimal mechanical strain,

uS Patent App. 11/020,910 (Jun. 22 2006).
[62] Harris K, Elias A, Chung H-J. Flexible electronics under strain: a review of mechanical characterization and durability enhancement strategies. J Mater Sci 2016;51(6):2771–805.
[63] Bartlett MD, Fassler A, Kazem N, Markvicka EJ, Mandal P, Majidi C. Stretchable, high-k dielectric elastomers through liquid-metal inclusions. Adv Mater 2016;28(19):3726–31.
[64] Mansy H, Grahe J, Sandler R. Elastic properties of synthetic materials for soft tissue modeling. Phys Med Biol 2008;53(8):2115.
[65] Park S, Mondal K, Treadway III RM, Kumar V, Ma S, Holbery JD, et al. Silicones for stretchable and durable soft devices: Beyond sylgard-184. ACS Appl Mater Interfaces 2018;10(13):11261–8.
[66] Ghaddar N, Ghali K, Chehaitly S. Assessing thermal comfort of active people in transitional spaces in presence of air movement. Energy Build 2011;43(10):2832–42.
[67] Leonov V. Thermoelectric energy harvesting of human body heat for wearable sensors. IEEE Sens J 2013;13(6):2284–91.
[68] Hyland M, Hunter H, Liu J, Veety E, Vashaee D. Wearable thermoelectric generators for human body heat harvesting. Appl Energy 2016;182:518–24.
[69] Settaluri KT, Lo H, Ram RJ. Thin thermoelectric generator system for body energy harvesting. J Electron Mater 2012;41(6):984–8.
[70] Jo S, Kim M, Kim M, Kim Y-J. Flexible thermoelectric generator for human body heat energy harvesting. Electron Lett 2012;48(16):1015–7.